

Sound propagation in periodic urban areas

Miguel Molerón, Simon Félix, Vincent Pagneux, and Olivier Richoux

Citation: *J. Appl. Phys.* **111**, 114906 (2012); doi: 10.1063/1.4725487

View online: <http://dx.doi.org/10.1063/1.4725487>

View Table of Contents: <http://jap.aip.org/resource/1/JAPIAU/v111/i11>

Published by the [American Institute of Physics](#).

Related Articles

Core loss behavior in high frequency high power transformers—I: Effect of core topology
J. Renewable Sustainable Energy **4**, 033112 (2012)

A divide and conquer real-space approach for all-electron molecular electrostatic potentials and interaction energies
J. Chem. Phys. **136**, 214104 (2012)

The design and analysis of beam-membrane structure sensors for micro-pressure measurement
Rev. Sci. Instrum. **83**, 045003 (2012)

Nanoscale temperature sensing using the Seebeck effect
J. Appl. Phys. **111**, 084306 (2012)

Study of second generation, high-temperature superconducting coils: Determination of critical current
J. Appl. Phys. **111**, 083902 (2012)

Additional information on *J. Appl. Phys.*

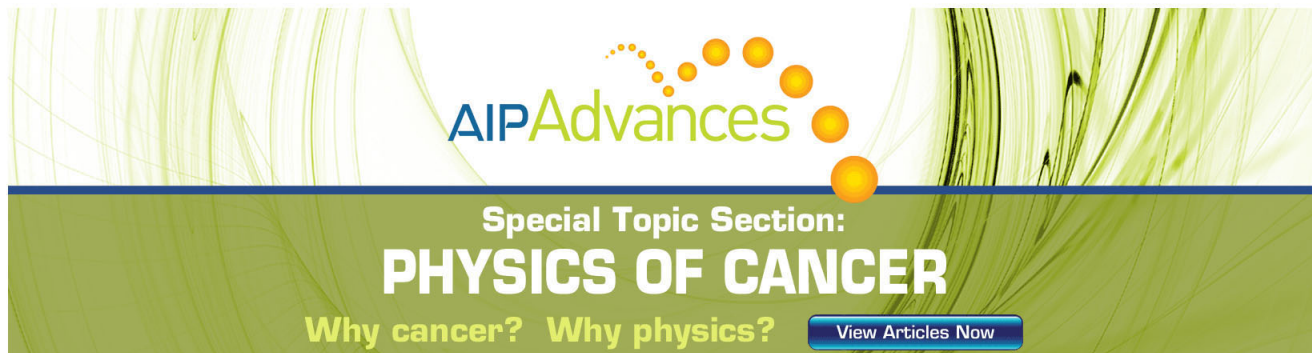
Journal Homepage: <http://jap.aip.org/>

Journal Information: http://jap.aip.org/about/about_the_journal

Top downloads: http://jap.aip.org/features/most_downloaded

Information for Authors: <http://jap.aip.org/authors>

ADVERTISEMENT



AIPAdvances

Special Topic Section:
PHYSICS OF CANCER

Why cancer? Why physics? [View Articles Now](#)

Sound propagation in periodic urban areas

Miguel Molerón, Simon Félix, Vincent Pagneux, and Olivier Richoux
 LAUM, CNRS, Université du Maine, Avenue Olivier Messiaen, 72085 Le Mans, France

(Received 20 January 2012; accepted 8 May 2012; published online 7 June 2012)

This paper presents an experimental and numerical study of low frequency sound propagation in regular urban areas, under the assumption of a periodic distribution of buildings. Although the radiation losses above the urban canyons are generally significant, our results show that the effects of the periodicity still occur. Band diagrams are notably characterized, both numerically and experimentally, to investigate the effect of the radiation above the periodic structure. The problem is tackled using a coupled modal-finite elements method. The main idea is to turn the original unbounded domain into an equivalent waveguiding structure, with PML bounding the originally open region. The experimental study is performed in a scale model of urban area. Numerical and experimental results on both the band diagrams and the wavefield propagating through the lattice are in good agreement. © 2012 American Institute of Physics. [<http://dx.doi.org/10.1063/1.4725487>]

I. INTRODUCTION

As a response to a growing social demand, the improvement of urban sound environment has become an important issue, arousing extensive researches in the last two decades.¹ Noise maps, that are now usual to determine and visualize the noise impact on the environment, necessitate a comprehensive modeling of the sound propagation in urban areas. Therefore, authors attempted to investigate the urban sound propagation, paying attention to the complexity of such a medium: irregular fades, interconnections with adjacent canyons, and large variety of materials and boundary conditions. Moreover, a predominant characteristic of the urban environment is the opening to the sky and the large radiative losses it induces.

If a large part of the papers concerns the propagation in a single urban canyon,^{2–4} few authors attempted to model the wave propagation in parallel or intersecting streets,^{5–11} or in larger urban areas,^{12–15} but often limited to 2D geometries.

In styling 3D extended distributions of buildings, the assumption of a periodic distribution is convenient to model the acoustic field, as much as it describes reasonably well some real situations. Doing this, it is possible to investigate the propagation through a large built area, while taking into account rigorously the three-dimensional characteristics of the problem, as the radiation above the streets.

Periodic media are known to exhibit peculiar properties (bandgaps, strong dispersion, anisotropy, and negative refraction) and have attracted a great deal of interest in electromagnetics and optics^{16,17} as, more recently, for acoustic and elastic waves.^{18–23} By assuming a periodic distribution of buildings in modeling the sound propagation in an urban environment, one may thus expect specific properties of periodic media to occur.

However, would these properties remain in the case (a lattice of open urban canyons) where important radiative losses are generally observed? This is the aim of the present work to investigate the competitive effects of the periodicity and the wave radiation.

In this paper, we investigate both experimentally and numerically the specific properties of open periodic lattices,

in particular, the presence of bandgaps. The experimental study is made using a 9×26 wooden cuboids lattice, the upper side of which is open. Using as a source a parametric antenna²⁴ that produces a directive plane wave in the audible frequency range, the transfer function of the lattice is measured. The numerical characterization of the open lattice is based on a FE-modal formulation of the wave propagation within open waveguiding structures, recently developed for the study of irregular canyons.²⁵ It basically consists in a finite element (FE) discretization of the problem in the transverse section of the waveguide (the street) with the open side artificially closed by perfectly matched layers (PML (Ref. 26)), and a multimodal formulation of the propagation in the longitudinal direction.

The paper is organized as follows. Section II shows the experimental device used in this work. Section III outlines the application of the modal-FE method to the study of periodic lattices. Two kinds of problems are treated: an infinite periodic lattice along one of the horizontal directions and an infinite periodic lattice along the two horizontal directions. In this section, some common issues on leaky modes and PML modes are discussed. Experimental and numerical results are presented in Sec. IV. The effect of the opening is evaluated by comparing the open lattice with an identical one, closed at the top with a rigid boundary. In the sequel, the open lattice is called OL and the closed one is called CL.

II. EXPERIMENTAL SETUP

A. Scale model of the urban area

The experimental device is shown in the Figure 1. Experiments are carried out in a semi-anechoic room. Walls are coated with a melamine foam, effective from 1 kHz onwards. The studied lattice is composed of 9×26 rectangular wooden cuboids with spatial periods $D_x = D_y = 7.5$ cm and obstacles dimensions $l_x \times l_y \times h = 5 \times 5 \times 15$ cm. Thus, the lattice has a total surface of 0.67×1.95 m² and the filling fraction is $ff = 44\%$. A screen is placed above the first row to avoid direct sound propagation from the source to the back of the

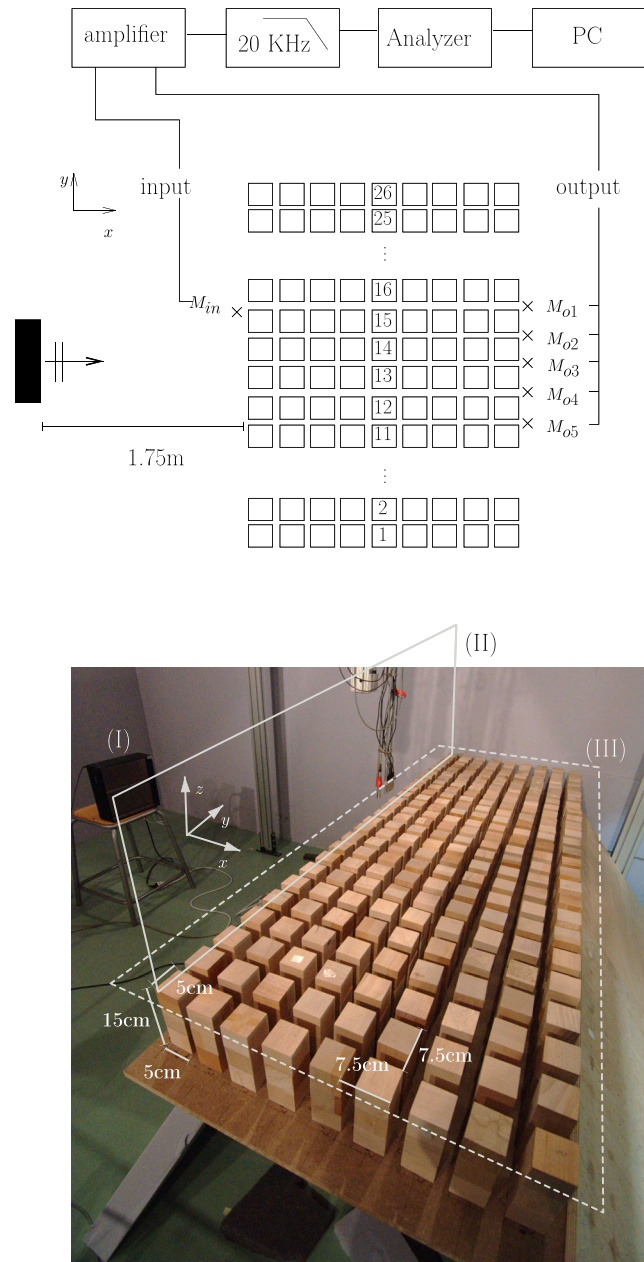


FIG. 1. Experimental setup. The top figure shows a schematic representation of the experimental setup. The parametric antenna is placed perpendicular to the lattice at the distance 1.75 m. Symbols “ \times ” represent microphones positions. The input pressure is measured at the position denoted by M_{in} . The output pressure is taken at five points behind the lattice, denoted by M_{o1} to M_{o5} , respectively. Signals are amplified and lowpass filtered to eliminate any remaining high frequency waves radiated by the source. The bottom figure shows a picture of the experimental device. Symbol (I) indicates the parametric antenna, (II) represents a screen permitting to avoid direct sound transmission over the lattice, and (III) indicates the covering used to obtain the CL.

lattice, which could distort the measurements. The CL is obtained by covering the OL with a wooden board, as indicated by the dashed rectangle in the Fig. 1.

B. Sound source

The lattice is excited using a parametric antenna model HSS (HyperSound Audio System), product from the American Technology Corporation. From an input signal at

frequency f_s , the source emits separately two high amplitude ultrasonic waves at frequencies f_1 and f_2 , related by $f_2 = f_1 + f_s$, with $f_1 = 47$ kHz. Then, due to non-linear interactions, new spectral components appear, among which are $f_1 - f_2$, $2f_1$, $f_1 + f_2$, $2f_2$. Because of the increase of attenuation with frequency, the difference frequency component $f_s = f_2 - f_1$ is predominant far from the source, while keeping the ultrasound properties. Thus, this device is able to deliver ultra-directive plane waves in the audible frequency range.

Fig. 2 shows the radiated field, measured at $f_s = 1.6$ kHz. The figure shows high frequency components in the near field, which vanishes approximately 1 m away from the source. Beyond this distance, only the difference frequency f_s remains, and it can be observed that wavefronts become plane.

Experiments have been performed by placing the antenna at 1.75 m from the lattice, and the source signal is a sweep sine from 1 to 8.3 kHz. To fix ideas, this would correspond to a few tens of a Hertz at “urban” scale. For instance, if the laboratory experiment corresponds to 1:100 scale, the frequency range at full scale would be 10 to 83 Hz. Such low frequency waves can be practically measured in urban environments as being produced by either heavy industrial machineries, intense impulse noise, or, for a part, the traffic noise,^{8,27} and they may propagate on long distances, compared with higher frequency waves.

C. Data acquisition

The acoustic pressure is measured using 1/2 in. microphones (B&K 4190), connected to a preamplifier (B&K 2669) and a conditioning amplifier (B&K Nexus 2669). Additionally, signals are lowpass filtered up to 20 kHz to eliminate any remaining high frequency component emitted by the source.

With the aim of detecting the bandgaps and passbands of the lattice, the transfer function between the output and the input pressures is measured. This parameter is determined by taking the averaged value of pressure at 5 output points, designed by M_{o1} to M_{o5} in Fig. 1. The input pressure is measured at the position denoted by M_{in} in the same figure. A single input point was found to be representative enough.

Wave field maps above the lattice have also been measured. In that case, the microphone position on a grid of measurement points is accurately controlled by a 3D robotic system. The spatial step is fixed to 20 points per wavelength. The acquisition of the acoustic pressure is performed using a sampling frequency $f_e = 20f_s$ (20 samples per period) during

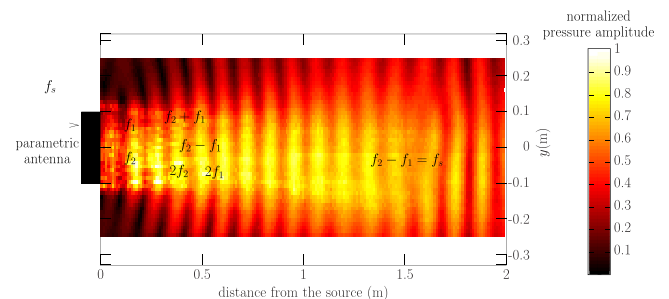


FIG. 2. Amplitude pressure map in the (x, y) plane radiated by the antenna.

a time length $T_e = N_e/f_e$, where $N_e = 2000$ (100 periods) is the number of samples. The RMS value of acoustic pressure is estimated by a least mean square method to determine the mean value, the amplitude, and the phase of the signal.

III. MODELING OF PERIODIC LATTICES USING THE MODAL-FE METHOD

A. The infinite periodic lattice along y

Consider the domain represented in Fig. 3(a). It consists in a finite series of periodic rows of rectangular cuboids, disposed along the y -direction. All the rows have the same spatial period D_y . The obstacles size and the distance between rows are arbitrary along the x -direction. Ω represents the whole domain and Γ designs the boundaries (obstacles and ground), which are assumed to be perfectly reflecting. To our purposes, the domain is closed at the top with a PML. Next, assuming a harmonic plane wave excitation, the Floquet-Bloch theorem imposes the following condition to the pressure field $p(x, y, z)$:

$$p(x, y + mD_y, z) = \exp(jmk\sin(\theta)D_y)p(x, y, z), \quad (1)$$

with $m \in \mathbb{Z}$, k the wavenumber, and θ the angle of incidence with respect to the x -axis. From Eq. (1), Ω can be reduced to the equivalent domain Ω_e , shown in the Fig. 3(b). This domain can be regarded as a piecewise constant waveguide, delimited at both sides by periodic boundaries Γ_L and Γ_R and at the top by the PML. This waveguide contains N_s straight segments with lengths $L^{(i)}$, $i = 1, \dots, N_s$, and two different cross-sections S_1 and S_2 .

The problem in Ω_e is written as

$$\begin{cases} (\Delta_\tau + k^2)p(x, y, z) = 0, \forall (x, y, z) \in \Omega_e, \\ \partial_n p(x, y, z) = 0, \forall (x, y, z) \in \Gamma, \\ p(x, y \in \Gamma_R, z) = \mu_y p(x, y \in \Gamma_L, z), \\ \partial_n p(x, y \in \Gamma_R, z) = -\mu_y \partial_n p(x, y \in \Gamma_L, z), \end{cases} \quad (2)$$

where ∂_n denotes the outward normal derivative with respect to the boundaries, $\mu_y = \exp(jk\sin(\theta)D_y)$ is the phase-shift imposed by the Floquet-Bloch theorem, and Δ_τ defined as

$$\Delta_\tau = \frac{\partial^2}{\partial x^2} + \frac{\partial^2}{\partial y^2} + \frac{1}{\tau} \frac{\partial}{\partial z} \left(\frac{1}{\tau} \frac{\partial}{\partial z} \right), \quad (3)$$

denotes the modified Laplacian operator which takes into account the PML. The coefficient τ of the PML is given by

$$\tau = \begin{cases} A \exp(j\beta), & \text{inside the PML,} \\ 1, & \text{elsewhere,} \end{cases} \quad (4)$$

with $A > 0$ and $0 < \beta < \pi/2$. The transverse problem is discretized using the FEM, and Eq. (2) are transformed into the matricial form

$$\vec{P}''(x) + (k^2 - \mathbf{M}_p^{-1} \mathbf{K}_p) \vec{P}(x) = \vec{0}, \quad (5)$$

where the n -th component of $\vec{P}(x)$ is the value of $p(x, y, z)$ at the node n and at the coordinate x : $P_n(x) = p(x, y_n, z_n)$, $n = 1, 2, \dots, N$, N being the number of nodes. The symbol $''$ represents the second derivative with respect to x , and $\mathbf{K}_p, \mathbf{M}_p$ are, respectively, the stiffness and mass matrices, resulting from the FEM discretization of the transverse differential operators (see Appendix A).

In each straight segment, a general solution of Eq. (5) can be found as a function of the eigenvalues α_n^2 and eigenvectors $\vec{\Phi}_n$ of the matrix $\mathbf{M}_p^{-1} \mathbf{K}_p$

$$\vec{P}^{(i)}(x) = \mathbf{\Phi} \left(\mathbf{D}(x) \vec{C}_1 + \mathbf{D}(L^{(i)} - x) \vec{C}_2 \right), \quad (6)$$

where $\mathbf{\Phi} = [\vec{\Phi}_1, \vec{\Phi}_2, \dots, \vec{\Phi}_N]$ is the eigenvectors matrix, $\mathbf{D}(x)$ is a diagonal matrix such that $D_{nn} = \exp(jk_{xn}x)$, with $k_{xn} = (k^2 - \alpha_n^2)^{1/2}$ the propagation constants, and vectors \vec{C}_1, \vec{C}_2 contain the unknowns modal amplitudes for forward and backward waves, respectively, which depend on the conditions at the extremities of the segments. To find these coefficients, the mode-matching method is used. The continuity equations for pressure and normal velocity are established at the waveguide discontinuities. Then, an output condition is defined by an admittance matrix \mathbf{Y} , fulfilling $\vec{U} = \mathbf{Y} \vec{P}$, with \vec{U} the x -component of the particle velocity on the basis of the interpolating polynomials used for the FEM computation. Later, using the continuity equations, the input and output admittance matrices of each straight segment are computed, step-by-step, from the output to the input segment. Finally, from a source condition, the wave field can be obtained at any point within the domain.²⁸⁻³⁰

B. The infinite periodic lattice along x and y

An infinite periodic lattice along x and y is now considered. A similar process as described in Duclos *et al.*²² is used to find the Bloch wavenumbers k_B . The application of the

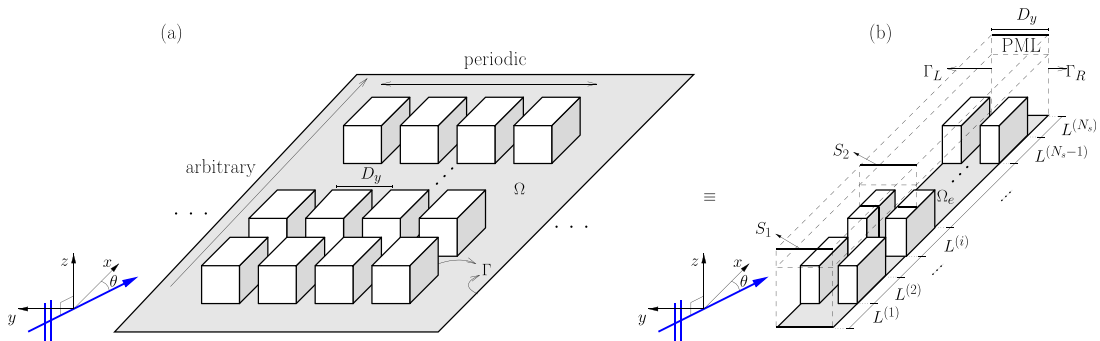


FIG. 3. (a) Geometry of the periodic lattice along y (b) unit cell of the lattice.

Floquet-Bloch theorem in both directions allows to reduce the domain to its unit cell represented in the Fig. 4. Then, using the mode-matching method, the scattering matrix \mathbf{S} of the unit cell, relating incident and scattered waves at the extremities, is obtained as

$$\begin{pmatrix} \vec{C}_b \\ \vec{C}_c \end{pmatrix} = \mathbf{S} \begin{pmatrix} \vec{C}_a \\ \vec{C}_d \end{pmatrix}, \quad (7)$$

where \mathbf{S} takes the form

$$\mathbf{S} = \begin{bmatrix} \mathbf{R} & \mathbf{T} \\ \mathbf{T} & \mathbf{R} \end{bmatrix}, \quad (8)$$

\mathbf{T} and \mathbf{R} being the transmission and reflection matrices, respectively. Additionally, the periodicity in the x -direction imposes the following condition to the amplitude coefficients:

$$\begin{pmatrix} \vec{C}_c \\ \vec{C}_d \end{pmatrix} = \mu_x \begin{pmatrix} \vec{C}_a \\ \vec{C}_b \end{pmatrix}, \quad (9)$$

with $\mu_x = \exp(jk_B D_x)$. Then, the combination of Eqs. (7) and (9) leads to the generalized eigenproblem

$$\begin{bmatrix} \mathbf{T} & \mathbf{R} \\ [0] & \mathbf{I} \end{bmatrix} \begin{pmatrix} \vec{C}_a \\ \vec{C}_d \end{pmatrix} = \mu_x \begin{bmatrix} \mathbf{I} & [0] \\ \mathbf{R} & \mathbf{T} \end{bmatrix} \begin{pmatrix} \vec{C}_a \\ \vec{C}_d \end{pmatrix}, \quad (10)$$

with $[0]$ the zero matrix and \mathbf{I} the identity matrix. Finally, the eigenvalues μ_x of this problem give the Floquet-Bloch wavenumbers k_B and the associated eigenvectors (\vec{C}_a, \vec{C}_d) contain the amplitude coefficients allowing to compute the wave field for each mode.

C. Modeling of closed lattices

Using the techniques described in Secs. III A and III B, the CL is modelled by replacing the PML termination at the

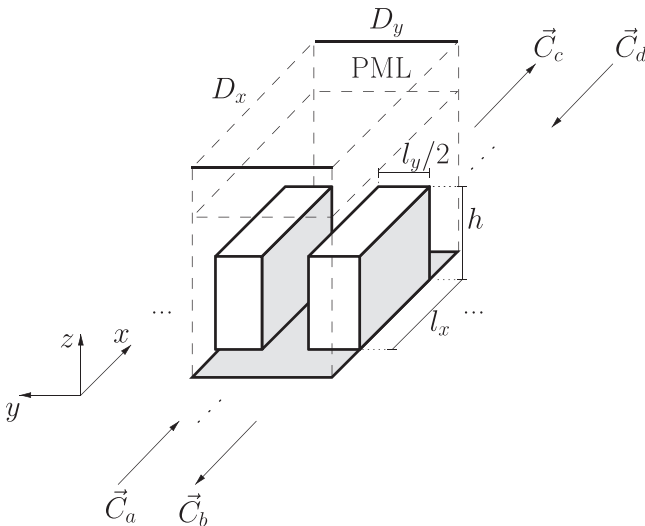


FIG. 4. Unit cell of the periodic lattice along x and y . The spatial periods are D_x and D_y . The obstacles length, width, and height are, respectively, denoted by l_x , l_y , and h .

top by a rigid boundary and considering $\tau = 1$ in the entire domain to obtain the classical Helmholtz equation.

D. On leaky modes and PML modes

When considering the CL, bandgaps, and propagative bands are represented by the solutions μ_x such that $\text{Im}\{k_B\} \neq 0$ and $\text{Im}\{k_B\} = 0$, respectively. In contrast, for the OL, all wavenumbers k_B are complex because of the radiation losses above the lattice. Such solutions represent the so-called leaky modes, modes that are partly propagated through the lattice and partly radiated towards the upper part (the Fig. 5(b) shows an example). A criterion for discriminate between bandgaps and propagative bands for the leaky modes can be defined by a threshold value η_0 of the loss factor

$$\eta = \left| \frac{\text{Im}\{k_B\}}{\text{Re}\{k_B\}} \right|, \quad (11)$$

from which a given solution can be considered, either propagative $\eta(k_B) < \eta_0$ or evanescent $\eta(k_B) > \eta_0$.

Additionally, with the introduction of PML, arises ‘‘PML’’ modes.^{31,32} These modes, strongly localized in the artificial absorbing layer (Fig. 5(b)), must be deleted, since they do not represent solutions of the original problem. Indeed, they are unphysical solutions of the equivalent PML problem. A useful criterion to separate PML modes and leaky modes was proposed by Shi *et al.*,³¹ based on the ratio E of the energy stored inside the PML volume V_{PML} to the energy stored in the total volume V_{tot} of the unit cell

$$E = \frac{\int_{V_{\text{PML}}} |p|^2 dV}{\int_{V_{\text{tot}}} |p|^2 dV}. \quad (12)$$

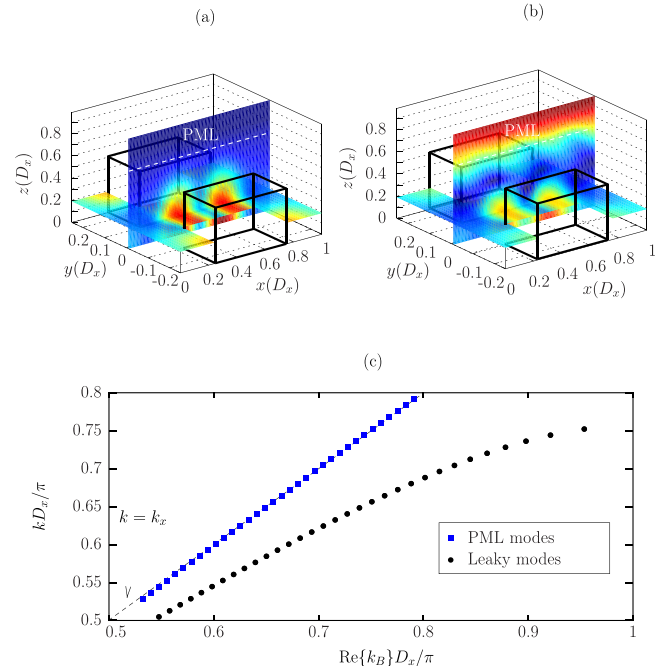


FIG. 5. (a) leaky mode, (b) PML mode, and (c) dispersion relation for the leaky (dots) and PML modes (squares) in normal incidence. Note that PML solutions matches the sound line $k = k_x$ (dashed line).

From Figs. 5(a) and 5(b), one should expect the ratio E to be close to zero for the leaky modes and much more important for the undesired PML modes.

The main drawback of such criterion is that E must be computed for each solution of Eq. (10), which considerably increases the computation time. However, a straightforward way to identify the PML modes comes from the fact that they mainly propagate in the free space above the periodic domain. As a consequence, they are almost independent of the geometry below them. Inversely, this does not happen with the leaky modes, whose behaviour is strongly related to the geometry of the periodic lattice. Then, for a given angle of incidence θ , the wavenumbers of PML modes lie close to a line defined by $k = k_x/\cos(\theta)$, called sound line and representing the dispersion relation of a plane wave propagating in the free space. This is illustrated by Fig. 5(c), where an arbitrary example of the dispersion relation of leaky and PML modes with normal incidence ($\theta = 0$) is represented. It is observed that the PML solutions matches the sound line, while the leaky mode dispersion relation is bended, influenced by the geometry of the periodic medium.

Note that the sound line is analogous to the light line for electromagnetic waves.^{31,33} This line can be regarded as the transition between evanescent and propagative leaky modes: assuming normal incidence ($k_y = 0$) and considering only the real part of k_B , the dispersion relation is approximated by $k^2 = (\text{Re}\{k_B\})^2 + k_z^2$. From this relation, it is deduced that, for modes above the sound line ($\text{Re}\{k_B\} < k$), the vertical component k_z of the wave vector is real. In other words, these modes are directed vertically, so radiated above the lattice. Modes coinciding with the sound line ($\text{Re}\{k_B\} = k$) represent waves propagating parallel to the horizontal plane and travelling at the speed of sound in free space. Finally, modes below the sound line ($\text{Re}\{k_B\} > k$) becomes evanescent along z and propagates along the x -direction with slight radiation losses defined by the imaginary part of k_B .

IV. RESULTS

A. Evaluation of the periodicity effects: Bandgaps in the lattice

Figs. 6(b) and 6(e) show the band structure in normal incidence for the CL and OL, respectively. For the later case, the threshold loss factor η_0 is adjusted to $\eta_0 = 0.1$ to filter the evanescent modes, and PML solutions has been eliminated.

In these figures, labels “mode ν ” denote the number ν of horizontal nodal lines of the mode: “mode 0” indicates 0 nodal lines; “mode 1,” 1 nodal line, and so on. Figs. 6(c) and 6(f) show the shape of modes 0, 1, and 2 at a given frequency for the CL and the OL, respectively (note that the shape of this modes varies with frequency, although it keeps the same number of horizontal nodal lines). For the CL, the cutoff frequencies of these modes can be obtained by solving the 1D Helmholtz problem along z with rigid boundary conditions. They are given by

$$f_\nu^{(CL)} = \frac{\nu c_0}{2h}.$$

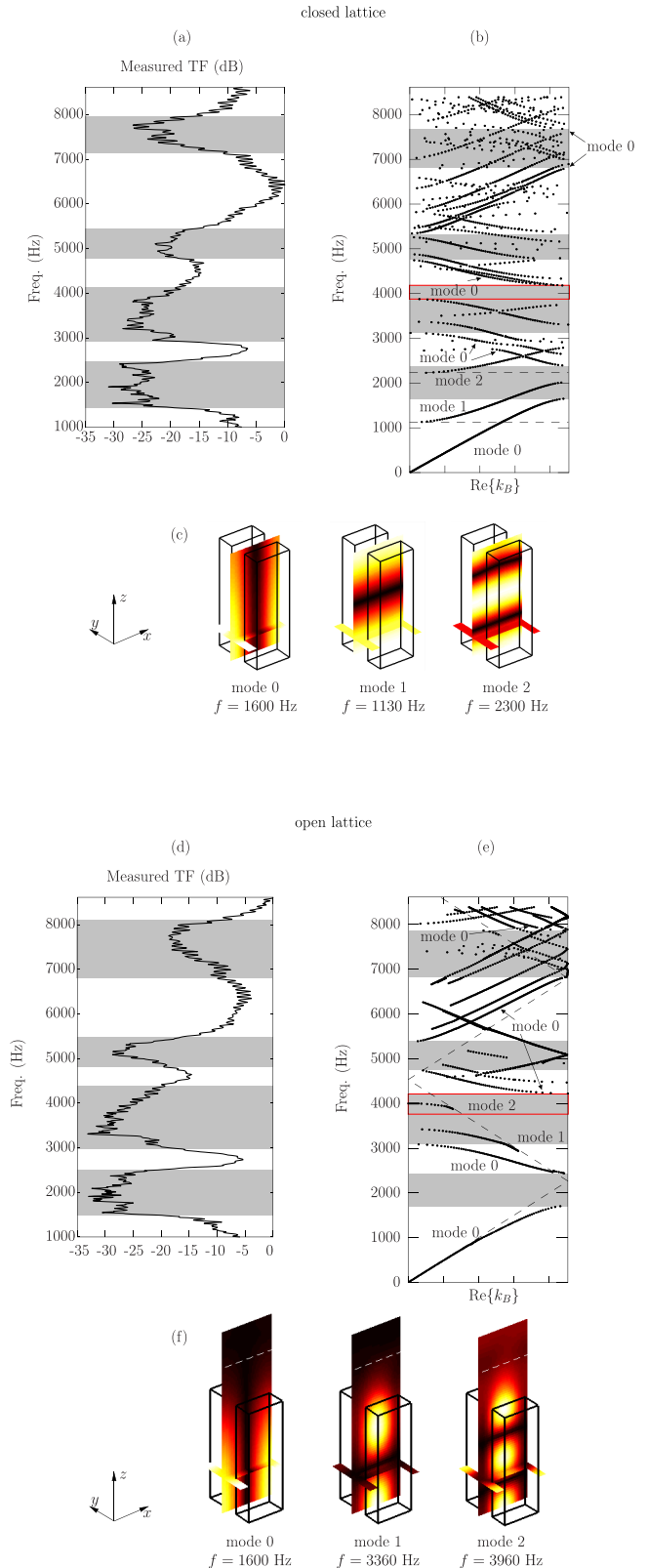


FIG. 6. (a) and (d) measured transfer functions. Curves are normalized to 0 dB for a more comfortable reading. Shaded zones indicates bandgaps; (b) and (e) band diagrams. Shaded zones indicate bandgaps for the mode 0; (c) and (f) shape of modes 0, 1, and 2 at a given frequency for the CL and OL, respectively.

Considering the sound speed $c_0 = 340 \text{ m s}^{-1}$, the first three frequencies are $f_{0,1,2}^{(CL)} = 0 \text{ Hz}, 1133 \text{ Hz}, \text{ and } 2267 \text{ Hz}$. They are represented by the dashed lines in Fig. 6(b). For the OL,

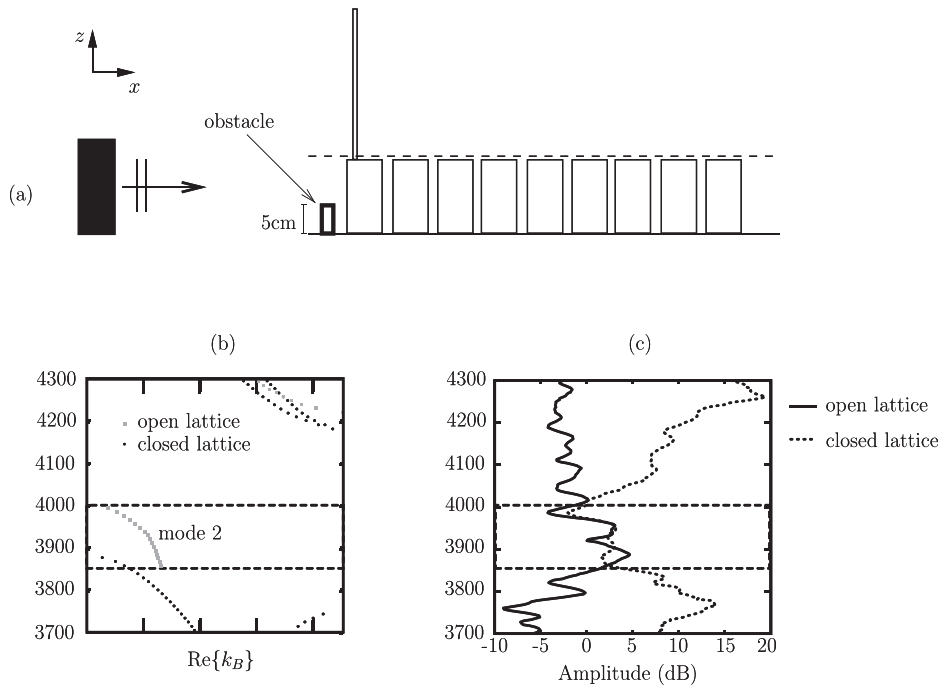


FIG. 7. (a) position of the obstacle in front of the lattice, used to activate higher order modes; (b) Band structure in the band 3.7 – 4.3 kHz for the CL (dots) and the OL (squares). (c) Measured transfer functions for the CL (dotted line) and the OL (continuous line). Note that in the band 3.85 – 4 kHz, no propagative modes exists in the CL, while the mode 2 emerges in the OL.

the cutoff frequencies of modes 0, 1, and 2 are determined by the sound line, represented by the oblique dashed line in Fig. 6(e).

Since, with the present configuration, the source impinges uniformly on the input cross-section of the lattices, one should expect that only the mode 0 will be excited. For this reason, the bandgaps for this mode have been highlighted, denoted by the shaded regions in Figs. 6(b) and 6(e). Four bandgaps are obtained in each case, defined in [1.65 – 2.39] kHz, [3.11 – 4.18] kHz, [4.72 – 5.36] kHz and [6.80 – 7.70] kHz for the CL and in [1.70 – 2.49] kHz, [3.09 – 4.23] kHz, [4.73 – 5.39] kHz, and [6.80 – 7.91] kHz for the OL. Note that the bandgaps positions for the mode 0 are quite similar in both cases.

Simulated results are compared to the experimental transfer functions shown in the Figs. 6(a) and 6(d). The curves for the OL and CL are quite similar. They also show four bandgaps, which are in good agreement with the computed band structures. Nevertheless, some differences in amplitude are visible. For instance, it can be observed that the first 3 bandgaps are more attenuated in the OL, while the fourth bandgap is more attenuated in the CL. This could be the result of a weak excitation of higher order modes, which could vary from one lattice to another. Comparing theoretical and experimental results, one observes that the measured bandgaps are in general wider, surely due to the inherent weak disorder and finite dimensions of the experimental lattice. Other dissipative effects, as the absorption of wood, may also play a role.

Regarding only the first mode, it can be concluded that the main factor governing the behaviour of this mode is the periodicity in the horizontal directions, while the condition at the top (closed or open) seems not to be relevant. In contrast, this does not happen with the higher order modes. Taking them into account, the presence of propagative modes is much more pronounced in the case of the CL. That seems

logical, since it is a lossless medium. However, an unexpected behaviour occurs in the frequency band 3.85–4 kHz. The Fig. 7(b) shows a zoom in this region of the band structure. It is observed that no propagative modes exist in the CL, while the mode 2 arises in the OL. To observe this phenomenon experimentally, the setup needs to be slightly modified. As mentioned before, with the present configuration, only the plane mode is supposed to be excited. In order to excite higher order modes, a bar of height 5 cm has been placed in front of the lattice (see Fig. 7(a)). With this configuration, the excitation is not plane anymore in the vertical direction z , so higher order modes are expected to be excited. The transfer functions are measured again in the frequency band 3.7 – 4.3 kHz, as shown in the Fig. 7(c). The curve of the CL shows a gap in the region 3.85 – 4 kHz, while the curve of the OL exhibits a slight bump, which agrees with the theoretical results.

The relevant point of this result is that the opening at the top can lead, at some frequencies, to a better propagation of waves, rather than their mitigation.

B. Pressure fields

The wave field in the horizontal plane 1 cm above the lattice, at 2 kHz, has been measured (Fig. 8(a)) and compared with the numerical field (Fig. 8(b)), computed with the technique explained in Sec. III A. The field is computed for a single period D_y , then repeated 6 times to give an overall result. As the excitation frequency is located in the first bandgap, fields exhibit a decay along the x -direction. Differences between the pressure fields are observed, which surely come from the non-uniformity of the experimental input signal, unlike the numerical excitation that equally extends over the y -direction. Also, the finite size and slight disorder of the experimental lattice may play a role. Despite the differences, both results seem to describe a similar global decay along x .

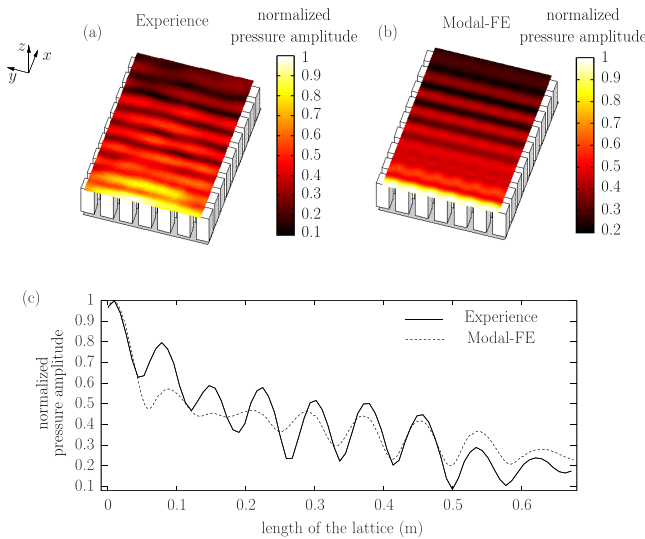


FIG. 8. (a) and (b) shows, respectively, the experimental and numerical horizontal planes of the pressure field at 2kHz, 1 cm above the lattice. (c) averaged pressure in the y -direction vs. x for the measured and the numerical fields.

To corroborate this, the mean value of pressure along the y -direction vs. x has been computed. Results are compared in the Fig. 8(c). Globally, both curves show a similar behaviour. Discrepancies are observed before the distance 0.3 m, where the position of the theoretical lobes is shifted and their amplitude varies significantly with respect to the experimental curve. The agreement is better from 0.3 m onwards.

V. CONCLUDING REMARKS

Open periodic lattices, of which a numerical and experimental study has been presented in this paper, can be regarded as idealized models of regular urban areas. By comparison of an open, two-dimensional, lattice with a more classical, closed, lattice, it has been shown that the band structure for the first propagating mode remains qualitatively the same when opening the upper part of the lattice. The measured transfer functions also are very similar in both cases. Thus, for a study involving only the first mode, the problem could be simplified to a 2D geometry by eliminating the vertical coordinate. In contrast, significant differences between the closed and the open lattice appear when higher order modes are included in the study. As it seems logical, the closed lattice exhibits a more pronounced presence of propagative modes. However, results have shown that this behaviour can be inverted at some frequencies. Unexpectedly, it is possible to find propagative bands in the open lattice that become evanescent in the closed one.

Compared with experiments, the modal-FE method predicts well the wave propagation in such domains. Although the present study is limited to an idealized geometry with normal incidence, the application to more complex and realistic building shapes as well as arbitrary angles of incidence is straightforward (see Refs. 11 and 25). Thus, this method can be used in future for a comprehensive evaluation of the influence of the urban morphology in low frequency sound propagation in urban areas.

ACKNOWLEDGMENTS

The authors would like to thank the council of the Région Pays de La Loire (France) for financial support. This work has also received support from the National Agency for Research (France) within the framework of the ANR Acou-Ville (ANR-09-JCJC-0009-01).

APPENDIX A: FEM COMPUTATION OF THE TRANSVERSE PERIODIC EIGENMODES

The aim of this section is to find the eigenfunctions and eigenvalues of the different cross-sections S_1, \dots, S_4 , shown in Figure 9. For each section, the eigenproblem is written as

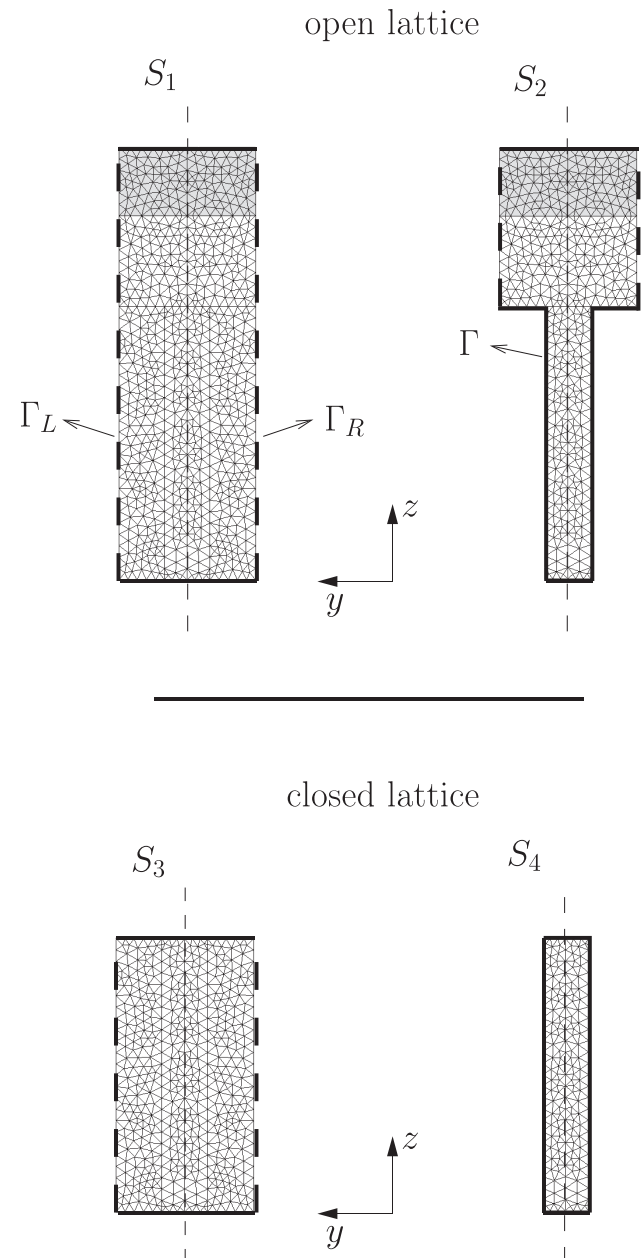


FIG. 9. Meshes examples of the transverse cross-sections of the lattices studied. Sections S_1 and S_2 are the cross-section of the open lattice. Sections S_3 and S_4 are the cross-sections of the closed one. Γ are perfectly reflecting boundaries, represented by the continuous thick lines. Γ_L and Γ_R are left and right periodic boundaries, represented by the dashed lines. The dashed thin line represents the vertical axis of symmetry.

$$\left(\frac{\partial^2}{\partial y^2} + \frac{1}{\tau} \frac{\partial}{\partial z} \left(\frac{1}{\tau} \frac{\partial}{\partial z}\right) + \alpha^2\right) \phi(y, z) = 0, \quad (\text{A1})$$

with the set of boundary conditions

$$\begin{cases} \partial_n \phi(y, z) = 0, \forall (y, z) \in \Gamma, \\ \phi(y \in \Gamma_R, z) = \mu_y \phi(y \in \Gamma_L, z), \\ \partial_n \phi(y \in \Gamma_R, z) = -\mu_y \partial_n \phi(y \in \Gamma_L, z), \end{cases} \quad (\text{A2})$$

where α , Γ , Γ_L , and Γ_R respectively denotes the in-plane wavenumber, perfectly reflecting boundaries, left and right periodic boundaries. For sections S_1 or S_2 , the parameter τ is defined by Eq. (4), while for sections S_3 or S_4 , $\tau = 1$ in the entire cross-section. The problem is discretized using linear triangular elements. The mesh generated satisfies two conditions: first, in order to fulfill the periodicity, nodes on Γ_R and Γ_L must be symmetrical with respect to the vertical axis of symmetry. Second, for a simplicity matter, the modal-FE method imposes an identical mesh in the matching section $S_1 \cap S_2$ for the OL, or $S_3 \cap S_4$ for the CL.²⁵

Then, the field $\phi(y, z)$ is developed on the basis of the interpolating polynomials $\psi_n(y, z)$ as

$$\phi(y, z) = \sum_{n=1}^N \Phi_n \psi_n = \vec{\psi} \vec{\Phi} \quad (\text{A3})$$

and the discretized problem takes the form

$$(\mathbf{K} - \alpha^2 \mathbf{M}) \vec{\Phi} = \vec{u}, \quad (\text{A4})$$

where \mathbf{K} and \mathbf{M} are the stiffness and mass matrix, respectively, defined by

$$K_{mn} = \int_{S_j} \frac{1}{\tau^2} \left(\frac{\partial \psi_m}{\partial y} \frac{\partial \psi_n}{\partial y} + \frac{\partial \psi_m}{\partial z} \frac{\partial \psi_n}{\partial z} \right) dydz \quad (\text{A5})$$

and

$$M_{mn} = \int_{S_j} \psi_m \psi_n dydz. \quad (\text{A6})$$

The vector \vec{u} is the contribution of the normal velocity at boundaries, which terms u_n is given by

$$u_n = \int_{\Gamma_{\text{tot}}} \partial_n \phi \psi_n d\Gamma_{\text{tot}}, \quad (\text{A7})$$

with $\Gamma_{\text{tot}} = \Gamma \cup \Gamma_L \cup \Gamma_R$. From Eq. (A7), it is deduced that this terms are equal to zero for all nodes except for those belonging to the periodic boundaries,

$$\begin{cases} u_n \neq 0, & \text{over } \Gamma_L \text{ and } \Gamma_R \\ u_n = 0, & \text{elsewhere.} \end{cases}$$

For the section S_4 , completely bounded by rigid walls, one has $\vec{u} = \vec{0}$ and the eigenmodes are found as the eigenvalues and eigenvectors of the matrix $\mathbf{M}^{-1} \mathbf{K}$ (see Eq. (A4)). For the rest, a similar technique as Allard *et al.*³⁴ to satisfy the periodic boundary conditions is used. To turn the notation on a more compact form, the matrix $\mathbf{D} = \mathbf{K} - \alpha^2 \mathbf{M}$ is defined and Eq. (A4) is rewritten as

$$\mathbf{D} \vec{\Phi} = \vec{u}. \quad (\text{A8})$$

Following, the problem is arranged so that nodes belonging to Γ_L (subscript L) appear first, followed by the internal ones (respectively I), and finally by those belonging to Γ_R (respectively R). The reordered problem is written as

$$\begin{pmatrix} \mathbf{D}_{LL} & \mathbf{D}_{LI} & \mathbf{D}_{LR} \\ \mathbf{D}_{IL} & \mathbf{D}_{II} & \mathbf{D}_{IR} \\ \mathbf{D}_{RL} & \mathbf{D}_{RI} & \mathbf{D}_{RR} \end{pmatrix} \begin{pmatrix} \vec{\Phi}_L \\ \vec{\Phi}_I \\ \vec{\Phi}_R \end{pmatrix} = \begin{pmatrix} \vec{u}_L \\ \vec{0} \\ \vec{u}_R \end{pmatrix}. \quad (\text{A9})$$

From Eqs. (A3) and (A7), the two last conditions of Eq. (A2) can be traduced by the vectorial expressions

$$\begin{cases} \vec{\Phi}_R = \mu_y \vec{\Phi}_L \\ \vec{u}_R = -\mu_y \vec{u}_L. \end{cases} \quad (\text{A10})$$

Next, introducing Eq. (A10) into Eq. (A9) and eliminating $\vec{\Phi}_R$ (or $\vec{\Phi}_L$) leads to the following eigenproblem for the remaining unknowns $\vec{\Phi}_L$ (or $\vec{\Phi}_R$) and $\vec{\Phi}_I$:

$$\mathbf{D}_p \begin{pmatrix} \vec{\Phi}_L \\ \vec{\Phi}_I \end{pmatrix} = \begin{pmatrix} \vec{0} \\ \vec{0} \end{pmatrix}, \quad (\text{A11})$$

with $\mathbf{D}_p = \mathbf{K}_p - \alpha^2 \mathbf{M}_p$

$$= \begin{bmatrix} \mathbf{D}_{LL} + \mu_y \mathbf{D}_{LR} + \mu_y^{-1} \mathbf{D}_{RL} + \mathbf{D}_{RR} & \mathbf{D}_{LI} + \mu_y^{-1} \mathbf{D}_{RI} \\ \mathbf{D}_{IL} + \mu_y \mathbf{D}_{IR} & \mathbf{D}_{II} \end{bmatrix}.$$

The eigenmodes are given by the eigenvalues α_n^2 and eigenvectors $(\vec{\Phi}_L, \vec{\Phi}_I)$ of the matrix $\mathbf{M}_p^{-1} \mathbf{K}_p$. Note that eliminated unknowns $\vec{\Phi}_R$ are straightforwardly given from relations (A10).

- ¹J. Kang, *Urban Sound Environment* (Taylor & Francis, London, 2007).
- ²O. Richoux, C. Ayrault, A. Pelat, S. Flix, and B. Lihoreau, *Appl. Acoust.* **71**, 731 (2010).
- ³A. Pelat, S. Félix, and V. Pagneux, *J. Acoust. Soc. Am.* **126**, 2864 (2009).
- ⁴J. Kang, *J. Acoust. Soc. Am.* **107**, 1394 (2000).
- ⁵J. Picaut, *Appl. Acoust.* **63**, 965 (2002).
- ⁶R. Bullen and F. Fricke, *J. Sound Vib.* **54**, 123 (1977).
- ⁷T. V. Renterghem, E. Salomons, and D. Botteldooren, *Appl. Acoust.* **67**, 487 (2006).
- ⁸A. Can, L. Leclercq, J. Lelong, and D. Botteldooren, *Appl. Acoust.* **71**, 764 (2010).
- ⁹M. Hornikx and J. Forssn, *J. Acoust. Soc. Am.* **122**, 2532 (2007).
- ¹⁰M. Hornikx and J. Forssn, *Appl. Acoust.* **72**, 665 (2011).
- ¹¹M. Molerón, S. Félix, V. Pagneux, J. Picaut, and O. Richoux, in *Proceedings of Internoise* (Lisbon, Portugal, 2010).
- ¹²J. Picaut, J. Hardy, and L. Simon, *Phys. Rev. E* **60**, 4851 (1999).
- ¹³D. G. Albert, L. Liu, and M. L. Moran, *J. Acoust. Soc. Am.* **118**, 616 (2005).
- ¹⁴D. G. Albert and L. Liu, *J. Acoust. Soc. Am.* **127**, 1335 (2010).
- ¹⁵D. Heimann, *Appl. Acoust.* **68**, 217 (2007).
- ¹⁶J. D. Joannopoulos, S. G. Johnson, J. N. Winn, and R. D. Meade, *Photonic Crystals: Molding the Flow of Light* (Princeton University Press, New Jersey, 2008).
- ¹⁷P. Markos and C. M. Soukoulis, *Wave Propagation: From Electrons to Photonic Crystals and Left-Handed Materials* (Princeton University Press, New Jersey, 2008).
- ¹⁸T.-C. Wu, T.-T. Wu, and J.-C. Hsu, *Phys. Rev. B* **79**, 104306 (2009).
- ¹⁹F. Wu, Z. Liu, and Y. Liu, *Phys. Rev. E* **66**, 046628 (2002).
- ²⁰J. O. Vasseur, P. A. Deymier, A. Khelif, P. Lambin, B. Djafari-Rouhani, A. Akjouj, L. Dobrzynski, N. Fettouhi, and J. Zemmouri, *Phys. Rev. E* **65**, 056608 (2002).

- ²¹X.-H. Wang, B.-Y. Gu, Z.-Y. Li, and G.-Z. Yang, *Phys. Rev. B* **60**, 11417 (1999).
- ²²A. Duclos, D. Lafarge, and V. Pagneux, *Eur. Phys. J.: Appl. Phys.* **45**, 1 (2009).
- ²³L. Feng, X.-P. Liu, M.-H. Lu, Y.-B. Chen, Y.-F. Chen, Y.-W. Mao, J. Zi, Y.-Y. Zhu, S.-N. Zhu, and N.-B. Ming, *Phys. Rev. B* **73**, 193101 (2006).
- ²⁴M. B. Bennett and D. T. Blackstock, *J. Acoust. Soc. Am.* **57**, 562 (1975).
- ²⁵A. Pelat, S. Félix, and V. Pagneux, *J. Acoust. Soc. Am.* **129**, 1240 (2011).
- ²⁶J.-P. Berenger, *J. Comput. Phys.* **114**, 185 (1994).
- ²⁷D. Ouis, *J. Environ. Psychol.* **21**, 101 (2001).
- ²⁸V. Pagneux, N. Amir, and J. Kergomard, *J. Acoust. Soc. Am.* **100**, 2034 (1996).
- ²⁹S. Félix and V. Pagneux, *J. Acoust. Soc. Am.* **116**, 1921 (2004).
- ³⁰S. Félix and V. Pagneux, *Wave Motion* **36**, 157 (2002).
- ³¹S. Shi, C. Chen, and D. W. Prather, *J. Opt. Soc. Am. A* **21**, 1769 (2004).
- ³²H. Rogier and D. De Zutter, *IEEE Trans. Microwave Theory Tech.* **49**, 712 (2001).
- ³³D. Sievenpiper, L. Zhang, R. Broas, N. Alexopolous, and E. Yablonovitch, *IEEE Trans. Microwave Theory Tech.* **47**, 2059 (1999).
- ³⁴J.-F. Allard, O. Dazel, G. Gautier, J.-P. Groby, and W. Lauriks, *J. Acoust. Soc. Am.* **129**, 1696 (2011).